On-Surface Synthesis of a Doubly Anti-Aromatic Carbon Allotrope: Cyclo[16]carbon

Yueze Gao,[1]† Florian Albrecht,[2]†, Igor Rončević,[1,4] Isaac Ettedgui,[1] Paramveer Kumar,[1] Lorel M. Scriven,[1] Kirsten E. Christensen,[1] Shantanu Mishra,[2] Luca Righetti,[3] Max Rossmannek,[3] Ivano Tavernelli,[3] Harry L. Anderson[1]* and Leo Gross[2]*

Affiliations:

[1] Department of Chemistry, Oxford University, Chemistry Research Laboratory; Oxford, United Kingdom.

[2] IBM Research Europe – Zürich, 8803 Rüschlikon, Switzerland.

[3] IBM Quantum, IBM Research – Zürich, 8803 Rüschlikon, Switzerland.

[4] Institute of Organic Chemistry and Biochemistry of the Czech Academy of Sciences; Prague, Czechia.

† These authors contributed equally.

*Corresponding authors. Email: harry.anderson@chem.ox.ac.uk; lgr@zurich.ibm.com

Abstract: Cyclocarbons are rings of carbon atoms, often formed as gas-phase carbon clusters. The only cyclocarbons yet to be well characterized are C_{10} and C_{18}, which are doubly aromatic with 4*n*+2 carbon atoms (where *n* is an integer), resulting in enhanced thermodynamic stability. Cyclocarbons with 4*n* atoms have been predicted to be less stable and doubly anti-aromatic. Here we report the first structural characterization of such a cyclocarbon, C_{16}, generated from $C_{16}(CO)_4Br_2$ on a NaCl surface. Atomic force microscopy (AFM) and scanning tunneling microscopy (STM) provide insight into the geometry and electronic structure, respectively, of neutral C_{16} and anionic C_{16}^{-}. We find that neutral C_{16} is circular, with significant bond-length alternation. This geometry confirms that it has an anti-aromatic ground state.

One-Sentence Summary: Despite being anti-aromatic, C_{16} was synthesized and characterized, revealing its anti-aromatic ground state and polyynic structure.

Main Text: The synthetic carbon allotropes graphene (*1*), carbon nanotubes (*2*) and fullerenes (*3*) have revolutionized materials science and led to new technologies. Recently, unconventional synthetic strategies such as dynamic covalent chemistry (*4*) and on-surface synthesis (*5*) have been used to create new forms of carbon, including γ-graphyne (*6*), covalent fullerene polymers (*7*), and biphenylene networks (*8*), as well as cyclo[10]carbon (*9*) and cyclo[18]carbon (*10*). Here we report the characterization of an anti-aromatic carbon allotrope, cyclo[16]carbon.

Cyclo[*N*]carbons are reactive carbon allotropes consisting of rings of *N* carbon atoms (*11, 12*). They are intermediates in the formation of fullerenes (*13*), and they constitute possible building blocks for other carbon allotropes such as graphyne (*14*). Many cyclocarbons (N = 6–40) have been detected in the gas-phase (*15*, *16*), and two examples (C_6 and C_8) have been trapped in solid argon and characterized by infrared spectroscopy (*17, 18*). The only cyclocarbons yet to have been synthesized in a condensed phase or definitively characterized are cyclo[10]carbon and cyclo[18]carbon. The 10- and 18-carbon rings were prepared on NaCl surfaces by atomic manipulation and characterized by scanning probe microscopy, revealing their cumulenic and polyynic structures, respectively (*9, 10, 19*). Cyclo[*N*]carbons with $N = 4n + 2$ (where n is an integer), such as C_{10} and C_{18}, are expected to be doubly aromatic and to have special stability, due to their closed-shell electronic configurations, relating to the presence of in-plane and out-of-plane aromatic Hückel circuits of $4n + 2$ π-electrons (*20–25*). In contrast, cyclo[4*n*]carbons have been predicted to be less stable and doubly anti-aromatic (*22–27*). This raises the question whether a cyclo[4*n*]carbon can be prepared and characterized. Here we report synthesis of the cyclo[4*n*]carbon C_{16} on a NaCl surface, together with its structural and electronic characterization by scanning probe microscopy, in different charge states. We demonstrate experimentally that C_{16} has strong bond-length alternation (BLA), and we show that this geometry implies that it is doubly anti-aromatic. Our experimental results are complemented by state-of-the-art quantum mechanical calculations, as well as by theoretical methods suitable for execution on a quantum computer.

Cyclocarbons have two orthogonal π-systems, one with orbitals in the ring plane and the other orthogonal to the ring plane. In an infinitely large cyclocarbon these two π-systems are degenerate, but in a finite ring, in-plane orbitals will be slightly higher in energy than their out-of-plane counterparts (*12*). This pattern of orbitals can lead to several possible electronic states. In the D_{16h} geometry of C_{16} with no BLA, the ground state may be a doubly aromatic |2200> state (Fig. 1, left), with 18 ($4n + 2$) and 14 ($4n – 2$) electrons in out-of-plane and in-plane π-systems, respectively. In this state, there are two degenerate pairs of frontier orbitals (out-of-plane A'' and B'' are occupied, and in-plane A' and B' are unoccupied). If we introduce BLA (D_{8h} symmetry), these orbital pairs will no longer be degenerate, with one member of each pair (A in Fig. 1, right) becoming stabilized relative to the other (B). This symmetry breaking leads to a doubly anti-aromatic |2020> configuration with 16 electrons in both in-plane and out-of-plane π-systems. A third possible state would be |1111>, with D_{16h} symmetry, but such open-shell configurations are known to be unstable relative to closed-shell alternatives (*28, 29*).

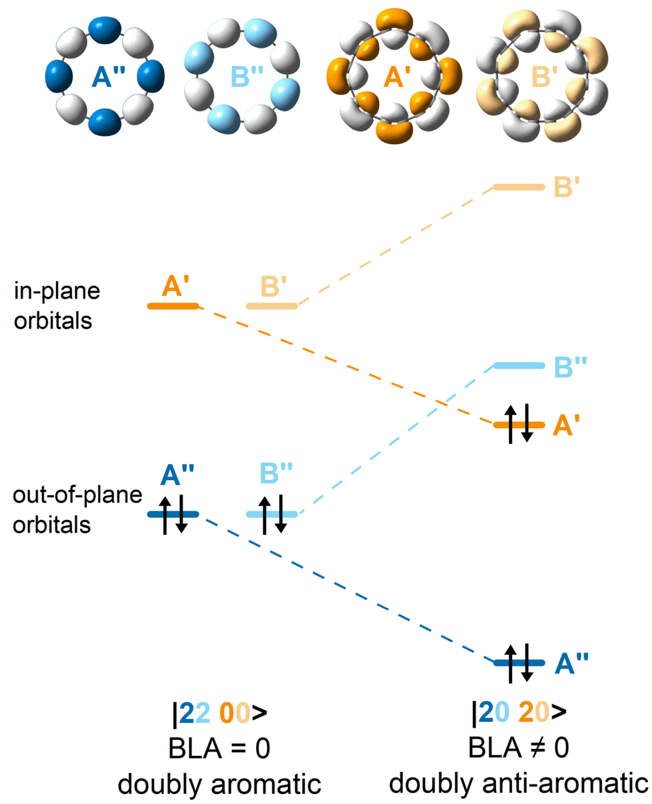

Fig. 1. Frontier orbitals of two electronic states of C_{16}. In-plane orbitals are labelled as A' and B', and out-of-plane orbitals as A" and B". Orbitals A', B' (and A", B") are related by a rotation and have equal energy when all bonds are of equal length. Introducing bond-length alternation lifts this degeneracy, resulting in orbital reordering and a doubly anti-aromatic ground state.

The unique structure, small size, and high symmetry of cyclocarbons has made them a target of many theoretical studies, which have sometimes produced conflicting results (*12*). Here, we investigate C_{16} using both state-of-the-art computational methods and a variational quantum eigensolver (*30*) paired with the quantum unitary coupled clusters singles doubles (q-UCCSD) (*31*) ansatz. These calculations confirm that the doubly anti-aromatic configuration, featuring strong BLA and consequent D_{8h} symmetry, is the ground state of C_{16}.

Results

Precursor synthesis: We explored two routes to C_{16}, as summarized in Fig. 2. Glaser-Hay coupling of a mixture of alkynes **1** and **2** gave macrocycle **3** in 20% yield. This macrocycle has a circuit of 16 sp^1 or sp^2 hybridized carbon atoms and it is anti-aromatic, in contrast to the corresponding C_{18}-precursor, which features a ring of 18 sp^1 or sp^2 hybridized carbon atoms and is aromatic. This difference in electronic structure is reflected by the ^{1}H NMR spectra and reactivities of these compounds (see fig. S1). Deprotection of **3** to give **4** proved difficult because of the high reactivity of these compounds (e.g., using concentrated sulfuric acid, as in case of C_{18}, was not viable). After testing many reaction conditions, we found that **3** can be converted to **4** using trifluoracetic acid containing water (2.5% by volume), but unfortunately the anti-aromatic cyclocarbon oxide **4** is too unstable for sublimation, preventing further work on this route to C_{16}. Glaser-Hay coupling of a mixture of compounds **1** and **5** gave the dibromo macrocycle **6** (20% yield), and the structure of this compound was confirmed by single-crystal X-ray diffraction (fig. S2). Deprotection of **6** with aqueous trifluoracetic acid gave **7** (94% yield). Although **7** is antiaromatic, like **4**, it is substantially more stable. At room temperature in the dark, solid samples of precursor **4** decompose to an extent of about 50% in 5 minutes, whereas under the same conditions, the extent of decomposition of **7** is only about 10% (fig. S3 and S4). The greater thermal stability of **7** made it possible to deposit this compound on a surface by sublimation under ultra-high vacuum.

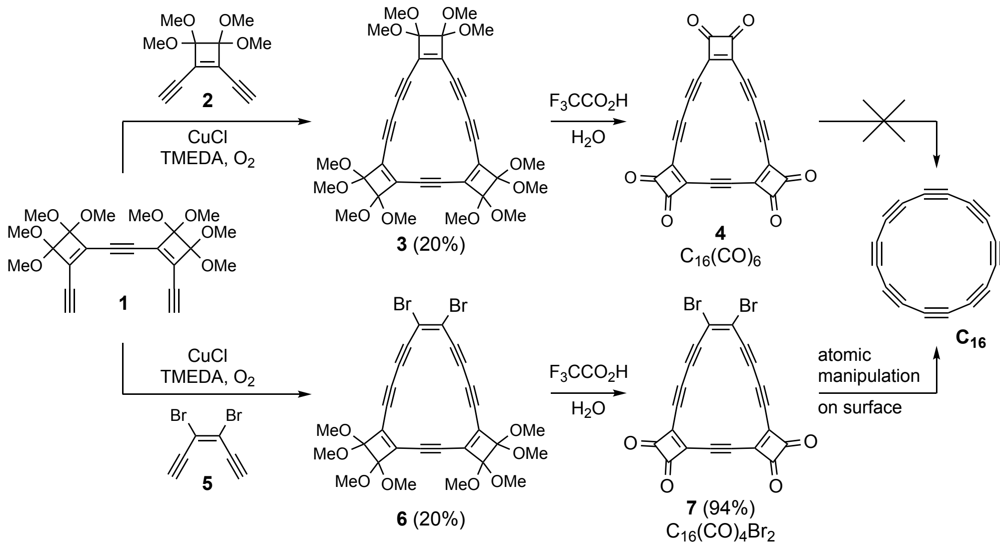

Fig. 2. Two approaches to the synthesis of C_{16}. The top route via **4** failed because this compound was found to be too unstable for sublimation.

On-surface synthesis and structural characterization: Precursor **7** was sublimed by fast heating from a Si wafer (*10*) onto a Cu(111) single crystal surface partially covered with bilayer NaCl, denoted as NaCl(2ML)/Cu(111), at a sample temperature of about $T = 10$ K. On-surface synthesis (Fig. 3A) and characterization by STM and AFM with CO tip functionalization (*32, 33*) were performed at $T = 5$ K. We found intact molecules of **7** on the NaCl(2ML)/Cu(111) surface, as shown in Fig. 3B. The Br atoms appear as bright (repulsive) dots in the AFM image (*19*), whereas the CO masking groups are dark features (*10*). The triple bonds show up as bright features, due to bond-order related contrast obtained with CO tip functionalization (*10, 33, 34*; for additional data on **7** see fig. S5).

Voltage pulses, applied from the tip above the molecules, were used to unmask individual molecules of precursor **7** by successively increasing the voltage. Debromination occurred at $V =$ 1.3–3.2 V, resulting in **8** (Fig. 3C; see fig. S6 for additional data). The CO masking groups dissociated at $V = 1.5$–3.3 V. Intermediate **9** was observed after dissociating the first pair of CO masking groups (Fig. 3D; see fig. S7 for additional data). Removal of a second pair of CO molecules gave the final product C_{16} (Fig. 3E, figs. S8, S9). Previously, gas-phase C_{16} has been formed from a molecular precursor (*35, 36*), and studied in its anionic (*36–38*) and cationic (*16, 39*) forms, but this is the first time C_{16} has been generated in a condensed phase. The yield for the on-surface synthesis of C_{16} was about 30%; in unsuccessful attempts, the ring opened to form linear polyynic chains (see fig. S10) or the molecule was picked up by the tip.

We observed C_{16} in two different forms on the NaCl surface (Fig. 3F,G) that we assign to neutral C_{16}^0 and negatively charged C_{16}^-, respectively (see also Fig. 4, figs. S11, S12). Whereas C_{16}^0 appears circular, C_{16}^- adopts a distorted oval geometry on defect-free NaCl. We observed a variety of adsorption sites for C_{16}^0 on the NaCl surface (fig. S13), indicating a weak interaction with the substrate. In contrast, C_{16}^- showed a systematic preference for adsorption above a bridge site (see figs. S14, S15). To investigate the interaction of C_{16}^0 and C_{16}^- with the NaCl surface, we performed DFT calculations with periodic boundary conditions. The calculated lowest-energy adsorption sites of C_{16}^{0} and C_{16}^{-} on NaCl are shown in Fig. 3H,I respectively. For the neutral charge state, we calculated an adsorption energy of 0.65 eV, which is similar to the value of 0.67 eV previously calculated for C_{18} on NaCl (*40*) that was predicted to diffuse readily across the surface. The calculated relaxed adsorption geometry of C_{16}^{-} on NaCl is oval shaped, with the molecule centered on a bridge site (Fig. 3I), in agreement with its experimentally observed site and shape (Fig. 3G, fig. S14 and Table S1). This adsorption geometry can be attributed to electrostatic interactions of the C_{16}^{-} anion with the Na cations and Cl anions, resulting in a significantly stronger adsorption energy (1.44 eV), compared to the neutral molecule.

The C_{16} molecules frequently moved on the surface during imaging with AFM and STM, indicating a small diffusion barrier and making it challenging to characterize them. To that end, the molecule was often moved close to a 3rd layer NaCl island, that provides a more stable adsorption site, facilitating detailed characterization. Fig. 3J-M show C_{16} adsorbed in a bay of a 3rd layer island imaged with AFM at different tip heights. Kelvin probe force spectroscopy (KPFS) confirmed that the molecule in Fig. 3F and J–M is charge neutral (Tables S2,S3 and fig. S16). The bright contrast obtained by CO-tip AFM above the triple bonds for larger tip heights (Fig. 3J,K) evolves to the shape of an octagon with corners at the positions of triple bonds at decreased tip heights (Fig. 3L,M). The results indicate BLA (*10*), i.e., a polyynic structure of neutral C_{16}.

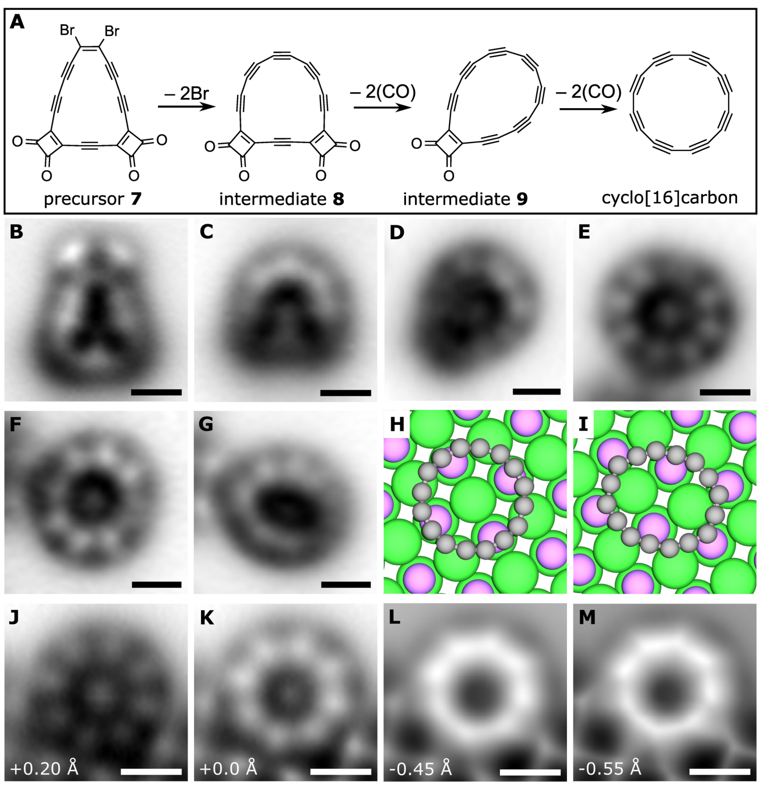

Fig. 3. On-surface synthesis of C_{16} and structural characterization. (A) reaction scheme. (B–E) Constant-height, CO-tip AFM images of precursor **7** (B), intermediates **8**, **9** (C, D) and C_{16} (E). Br atoms were dissociated by voltage pulses applied above the molecule, with $V = 1.3$–3.2 V. CO masking groups were dissociated with $V = 1.5$–3.3 V. (F-I) AFM image of C_{16} in neutral (F) and anionic (G) charge state, and calculated lowest-energy adsorption sites of C_{16}^{0} (H) and C_{16}^{-} (I) on NaCl. (J–M) C_{16}^{0} adsorbed in a bay of a 3rd layer NaCl island, imaged with AFM at different tip heights. All molecules are adsorbed on NaCl(2ML)/Cu(111). The tip-height offsets provided in the images refer the STM setpoint of $I = 0.2$ pA and $V = 0.2$ V on bare NaCl(2ML)/Cu(111). Scale bars 0.5 nm.

Charge state switching and electronic characterization: The charge state of C_{16} can be controllably switched using the applied bias, as shown in Fig. 4. At about $V = 0.5$ V, the molecule switched from neutral C_{16}^{0} to the anion C_{16}^{-}, (and at $V = -0.3$ V in the reverse direction, C_{16}^{-} to C_{16}^{0}, see figs. S11, S17). The STM images in Fig. 4A,B show C_{16}^{0} and C_{16}^{-}, respectively. The negative charge state leads to a characteristic dark halo (Fig. 4B) and interface state scattering as observed in the difference image Fig. 4C (*41*), see also fig. S11 for images with enhanced contrast. The assignments of these charge states are corroborated by KPFS, see fig. S17. AFM data for C_{16}^{0} and C_{16}^{-} are shown in Fig. 4D,E with corresponding Laplace filtered data in Fig. 4G,H, respectively. In this case, the structural distortion of C_{16}^{0} and C_{16}^{-} is similar, which we assign to the influence of the adjacent 3rd layer NaCl island.

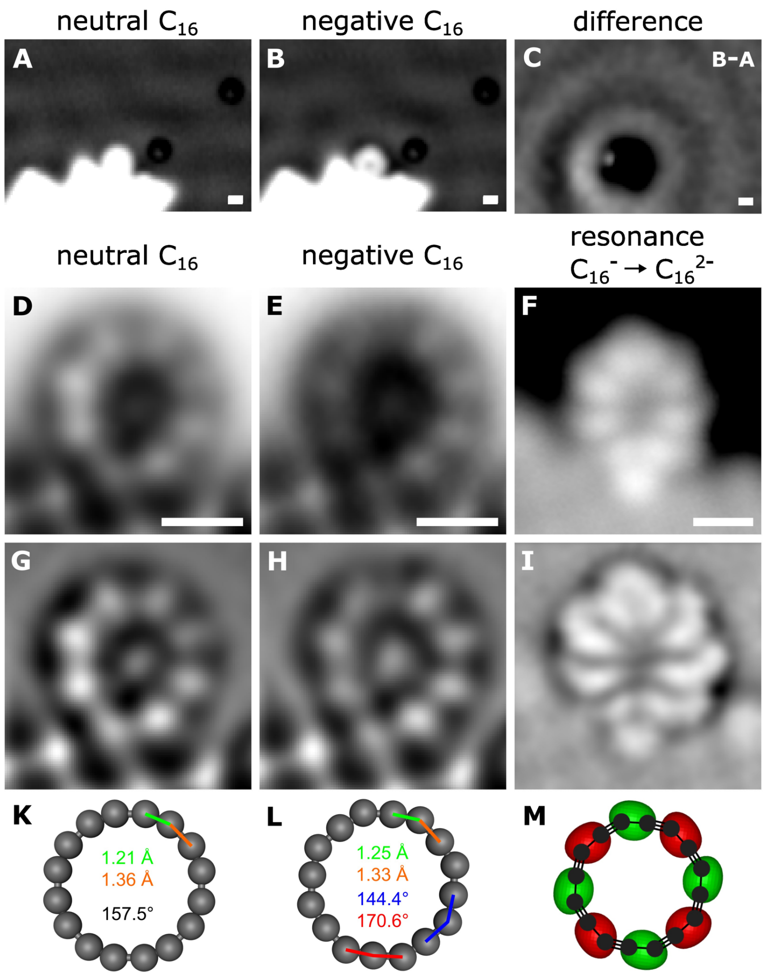

Fig. 4. Charge-state switching and electronic characterization. (A, B) Constant-current STM images of C_{16} in neutral and negative charge state, respectively ($V = 50$ mV, $I = 0.2$ pA). (C) Difference of panels B and A. (D, E) Constant-height AFM images of C_{16}^{0} and C_{16}^{-}, respectively. (F) Const.-current STM ($I = 0.4$ pA and $V = +1.2$ V) mapping the ionic resonance of C_{16}^{-} to C_{16}^{2-}. (G–I) Same data as (D–F) after applying a Laplace filter. The molecule was adsorbed on NaCl(2ML)/Cu(111), near a 3rd layer island. All scale bars 0.5 nm. (K, L) Optimized geometries (ωB97XD/def2-TZVP) of C_{16}^{0} and C_{16}^{-}, respectively, with bond lengths and bond angles indicated. (M) Simulated isosurface at 0.2 a.u. (1.4 e/Å^3) of the LUMO of C_{16}^{-}.

The more stable adsorption at the 3rd layer island allowed us to image the molecule at increased bias voltages without inducing movement of the molecule. At about 1.2 V, we observe the onset of an electronic resonance by scanning tunneling spectroscopy (STS; see fig. S17). The STM image at 1.2 V shown in Fig. 4F (Laplace filtered data in Fig. 4I), reveals the orbital density corresponding to that resonance (*42*). As the molecule is already in the anionic charge state at V > 0.5 V, we assign this resonance to the transition from anionic C_{16}^{-}, to the dianionic charge state C_{16}^{2-}, giving us insight into the electronic structure of C_{16}.

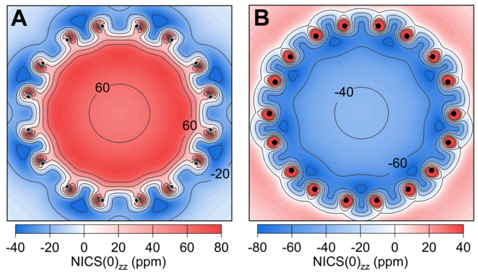

Fig. 5. Nucleus independent shift. $NICS(0)_{zz}$ plots for (A) neutral C_{16} and (B) C_{18} (ωB97XD/def2-TZVP).

Multireference methods and DFT (see Tables S4 and S5 for details) both predict C_{16}^{0} to have a |2020> ground state with a polyynic geometry and significant BLA, but no bond-angle alternation (BAA), resulting in D_{8h} symmetry (Fig. 4K). In contrast, C_{16}^{-} shows both BLA and BAA (Fig. 4L), i.e., an additional symmetry breaking to C_{8h}. The electronic structure of C_{16}^{0} (Fig. 1 right and fig. S18) features a nearly degenerate pair of occupied molecular orbitals A'' (HOMO–1) and A' (HOMO), as well a nearly degenerate pair of unoccupied molecular orbitals B'' (LUMO) and B' (LUMO+1); in both pairs, the in-plane orbital has a slightly higher energy than the out-of-plane one. HOMO and LUMO+1 (as well as HOMO–1 and LUMO) are related by rotation (see |2020> configuration on Fig. 1), giving rise to a strongly paratropic ring current (*43*), calculated to be 25 nA/T; see SI. This ring current is reflected by the pattern of shielding and deshielding, visualized using the nucleus independent chemical shift (NICS, Fig 5A), which is opposite to the pattern for aromatic C_{18} (Fig. 5B). In the C_{16}^{-} anion, single occupation of the B'' LUMO leads to a symmetry lowering and BAA. The DFT-predicted LUMO of C_{16}^{-} (Fig. 4M, fig. S19) can be compared to the electronic resonance imaged by STM (Fig. 4F,I), which corresponds to the squared orbital wavefunction (*42*) and to the addition of a second electron to the singly occupied out-of-plane orbital (B'') in C_{16}^{-}. Both theory and experiment show high-density lobes above the long bonds of C_{16}^{-}, which are located between the bright features of the corresponding AFM images. The symmetry lowering from D_{8h} to C_{8h} in C_{16}^{-}, that is the effect of BAA, is reflected in the shape of the orbital lobes and can be observed in both experiment (Fig. 4F,I) and theory (Fig. 4M).

AFM data showing BLA, and STM data showing the orbital density for the C_{16}^{-} to C_{16}^{2-} transition, corresponding to addition of an electron to the B'' orbital of C_{16}^{-}, are all in excellent agreement with the calculations, strongly suggesting the doubly anti-aromatic character of C_{16}^{0}, which causes pronounced BLA and a D_{8h} geometry. The two other possible electronic configurations of C_{16}, |2200> and |1111>, were calculated by DFT to have nearly identical D_{16h} minima with no BLA and significantly higher energies (2.47 and 1.78 eV, respectively) than the doubly anti-aromatic |2020>. Relative ground-state energies of the D_{8h} and D_{16h} minima were also determined using q-UCCSD, by simulating quantum circuits with Qiskit (*44*). Q-UCCSD predicts that the D_{8h} minimum is more stable than the D_{16h} one by 3.38 eV, which is very similar to the result obtained using conventional coupled clusters singles doubles (3.31 eV; see SI for further discussion).

Our experimental results, most importantly the observed BLA for neutral C_{16}, confirm the occupation of both π-systems with 16 electrons (in-plane and out-of-plane), making the molecule doubly anti-aromatic. In addition, NICS and bond current calculations on neutral C_{16} indicate significant anti-aromaticity in this electronic configuration. The investigation of both C_{16}^{0} and C_{16}^{-} provides confidence in the assignment of charge states and insights into the electronic structure of the molecule. The synthesis, stabilization and characterization of C_{16} opens the way to create other elusive carbon-rich anti-aromatic molecules by atom manipulation. The high reactivity of C_{16}, and other cyclocarbons, renders them promising precursors to novel carbon allotropes (*14*).

References and Notes

[1] K. S. Novoselov, A. K. Geim, S. V. Morozov, D. Jiang, Y. Zhang, S. V. Dubonos, I. V. Grigorieva, A. A. Firsov, Electric field effect in atomically thin carbon films. *Science* **306**, 666–669 (2004).

[2] S. Iijima, T. Ichihashi, Single-shell carbon nanotubes of 1-nm diameter. *Nature* **363**, 603–605 (1993).

[3] H. W. Kroto, J. R. Heath, S. C. O'Brien, R. F. Curl, R. E. Smalley, C_{60}: Buckminsterfullerene. *Nature* **318**, 162–163 (1985).

[4] S. Clair, D. G. de Oteyza, Controlling a chemical coupling reaction on a surface: tools and strategies for on-surface synthesis. *Chem. Rev.* **119**, 4717–4776 (2019).

[5] C. S. Diercks, O. M. Yaghi, The atom, the molecule, and the covalent organic framework. *Science* **355**, eaal1585 (2017).

[6] Y. Hu, C. Wu, Q. Pan, Y. Jin, R. Lyu, V. Martinez, S. Huang, J. Wu, L. J. Wayment, N. A. Clark, M. B. Raschke, Y. Zhao, W. Zhang, Synthesis of γ-graphyne using dynamic covalent chemistry. *Nat. Synth.* **1**, 449–454 (2022).

[7] E. Meirzadeh, A. M. Evans, M. Rezaee, M. Milich, C. J. Dionne, T. P. Darlington, S. Tong Bao, A. K. Bartholomew, T. Handa, D. J. Rizzo, R. A. Wiscons, M. Reza, A. Zangiabadi, N. Fardian-Melamed, A. C. Crowther, P. J. Schuck, D. N. Basov, X. Zhu, A. Giri, P. E. Hopkins, P. Kim, M. L. Steigerwald, J. Yang, C. Nuckolls, X. Roy, A few-layer covalent network of fullerenes. *Nature* **613**, 71–76 (2023).

[8] Q. Fan, L. Yan, M. W. Tripp, O. Krejčí, S. Dimosthenous, S. R. Kachel, M. Chen, A. S. Foster, U. Koert, P. Liljeroth, J. M. Gottfried, Biphenylene network: A nonbenzenoid carbon allotrope. *Science*. **372**, 852–856 (2021).

[9] W. Xu, L. Sun, W. Gao, F. Kang, M. Zhao, An annular carbon allotrope, cumulenic cyclo[10]carbon. *Research Square* DOI: https://doi.org/10.21203/rs.3.rs-2616838/v1 (2023).

[10] K. Kaiser, L. M. Scriven, F. Schulz, P. Gawel, L. Gross, H. L. Anderson, An sp-hybridized molecular carbon allotrope, cyclo[18]carbon. *Science* **365**, 1299–1301 (2019).

[11] Y. Tobe, T. Wakabayashi, In *polyynes: synthesis, properties, and applications*; F. Cataldo, Ed.; CRC Press/Taylor & Francis: Boca Raton, p. 99 (2006).

[12] H. L. Anderson, C. W. Patrick, L. M. Scriven, S. L. Woltering, A short history of cyclocarbons. *Bull. Chem. Soc. Jpn.* **94**, 798–811 (2021).

[13] G. von Helden, N. G. Gotts, M. T. Bowers, Experimental evidence for the formation of fullerenes by collisional heating of carbon rings in the gas phase. *Nature* **363**, 60–63. (1993).

[14] F. Diederich, Carbon scaffolding: building acetylenic all-carbon and carbon-rich compounds. *Nature* **369**, 199 (1994).

[15] K. S. Pitzer, E. Clementi, Large molecules in carbon vapor. *J. Am. Chem. Soc.* **81**, 4477–4485 (1959).

[16] S. J. P. Marlton, J. T. Buntine, P. Watkins, C. Liu, U. Jacovella, E. Carrascosa, J. N. Bull, E. J. Bieske, Probing colossal carbon rings. *J. Phys. Chem. A* **127**, 1168–1178 (2023).

[17] S. L. Wang, C. M. L. Rittby, W. R. M. Graham, Detection of cyclic carbon clusters. I. Isotopic study of the $\nu_4(e')$ mode of cyclic C_6 in solid Ar. *J. Chem. Phys.* **107**, 6032–6037 (1997).

[18] S. L. Wang, C. M. L. Rittby, W. R. M. Graham, Detection of cyclic carbon clusters. II. Isotopic study of the $\nu_{12}(e_u)$ mode of cyclic C_8 in solid Ar. *J. Chem. Phys.* **107**, 7025–7033 (1997).

[19] L. M. Scriven, K. Kaiser, F. Schulz, A. J. Sterling, S. L. Woltering, P. Gawel, K. E. Christensen, H. L. Anderson, L. Gross, Synthesis of cyclo[18]carbon *via* debromination of $C_{18}Br_6$. *J. Am. Chem. Soc.* **142**, 12921–12924 (2020).

[20] F. Diederich, Y. Rubin, C. B. Knobler, R. L. Whetten, K. E. Schriver, K. N. Houk, Y. Li, All-carbon molecules: Evidence for generation of cyclo[18]carbon from a stable organic precursor. *Science* **245**, 1088–1090 (1989).

[21] P. v. R. Schleyer, H. Jiao, M. N. Glukhovtsev, J. Chandrasekhar, E. Kraka, Double aromaticity in the 3,5-dehydrophenyl cation and in cyclo[6]carbon. *J. Am. Chem. Soc.* **116**, 10129–10134 (1994).

[22] P. W. Fowler, N. Mizoguchi, D. E. Bean, R. W. A. Havenith, Double aromaticity and ring currents in all-carbon rings. *Chem. Eur. J.* **15**, 6964–6972 (2009).

[23] N. D. Charistos, A. Muñoz-Castro, Induced magnetic field in sp-hybridized carbon rings: analysis of double aromaticity and antiaromaticity in cyclo[2*N*]carbon allotropes. *Phys. Chem. Chem. Phys.* **22**, 9240–9249 (2020).

[24] G. V. Baryshnikov, R. R. Valiev, R. T. Nasibullin, D. Sundholm, T. Kurten, H. Ågren, Aromaticity of even-number cyclo[*n*]carbons. *J. Phys. Chem. A* **124**, 10849−10855 (2020).

[25] J. Hutter, H. P. Lüthi, F. Diederich, Structures and vibrational frequencies of the carbon molecules C_2-C_{18} calculated by density functional theory. *J. Am. Chem. Soc.* **116**, 750–756 (1994).

[26] K. Ohno, Quantum chemical exploration of conversion pathways and isomeric structures of C_{16} molecules. *Chem. Phys. Lett.* **711**, 60–65 (2018).

[27] E. J. Bylaska, R. Kawai, J. H. Weare, From small to large behavior: The transition from the aromatic to the Peierls regime in carbon rings. *J. Chem. Phys.* **113**, 6096–6106 (2000).

[28] P. G. Wenthold, D. A. Hrovat, W. T. Borden, W. C. Lineberger, Transition-state spectroscopy of cyclooctatetraene. *Science* **272**, 1456–1459 (1996).

[29] P. B. Karadakov, Aromaticity and antiaromaticity in the low-lying electronic states of cyclooctatetraene. *J. Phys. Chem. A* **112**, 12707–12713 (2008).

[30] A. Peruzzo *et al.*, A variational eigenvalue solver on a photonic quantum processor. *Nat. Commun.* **5**, 4213 (2014).

[31] P. K. Barkoutsos, J. F. Gonthier, I. Sokolov, N. Moll, G. Salis, A. Fuhrer, M. Ganzhorn, D. J. Egger, M. Troyer, A. Mezzacapo, S. Filipp, I. Tavernelli, Quantum algorithms for electronic structure calculations: particle-hole Hamiltonian and optimized wave-function expansions. *Phys. Rev. A* **98**, 022322 (2018).

[32] L. Gross, F. Mohn, N. Moll, P. Liljeroth, G. Meyer, The chemical structure of a molecule resolved by atomic force microscopy. *Science* **325**, 1110–1114 (2009).

[33] L. Gross, F. Mohn, N. Moll, B. Schuler, A. Criado, E. Guitián, D. Peña, A. Gourdon, G. Meyer, Bond-order discrimination by atomic force microscopy. *Science* **337**, 1326–1329 (2012).

[34] N. Pavliček, P. Gawel, D. R. Kohn, Z. Majzik, Y. Xiong, G. Meyer, H. L. Anderson, L. Gross, Polyyne formation via skeletal rearrangement induced by atomic manipulation. *Nat. Chem.* **10**, 853–858 (2018).

[35] Y. Tobe, H. Matsumoto, K. Naemura, Y. Achiba, T. Wakabayashi, Generation of cyclocarbons with 4*n* carbon atoms (C_{12}, C_{16}, and C_{20}) by [2 + 2] cycloreversion of propellane-annelated dehydroannulenes. *Angew. Chem. Int. Ed. Engl.* **35**, 1800–1802 (1996).

[36] T. Wakabayashi, M. Kohno, Y. Achiba, H. Shiromaru, T. Momose, T. Shida, K. Naemura, Y. Tobe, Photoelectron spectroscopy of C_n^- produced from laser ablated dehydroannulene derivatives having carbon ring size of n = 12, 16, 18, 20, and 24. *J. Chem. Phys.* **107**, 4783–4787 (1997).

[37] S. Yang, K. J. Taylor, M. J. Craycraft, J. Conceicao, C. L. Pettiette, O. Cheshnovsky, R. E. Smalley, UPS of 2–30-atom carbon clusters: chains and rings. *Chem. Phys. Lett.* **144**, 431–436 (1988).

[38] M. Ohara, D. Kasuya, H. Shiromaru, Y. Achiba, Resonance-enhanced multiphoton electron detachment (REMPED) study of carbon anions up to C_{21}^-. *J. Phys. Chem. A* **104***,* 8622–8626 (2000).

[39] G. von Heiden, M.-T. Hsu, P. R. Kemper, M. T. Bowers, Structures of carbon cluster ions from 3 to 60 atoms: Linears to rings to fullerenes. *J. Chem. Phys.* **95**, 3835–3837 (1991).

[40] G. V. Baryshnikov, R. R. Valiev, A. V. Kuklin, D. Sundholm, H. Ågren, Cyclo[18]carbon: insight into electronic structure, aromaticity, and surface coupling. *J. Phys. Chem. Lett.* **10**, 6701−6705 (2019).

[41] J. Repp, G. Meyer, F. E. Olsson, M. Persson, Controlling the charge state of individual gold adatoms. *Science* **305**, 493–495 (2004).

[42] J. Repp, G. Meyer, S. M. Stojkovic, A. Gourdon, C. Joachim, Molecules on insulating films: Scanning-tunneling microscopy imaging of individual molecular orbitals. *Phys. Rev. Lett.* **94**, 26803 (2005).

[43] E. Steiner, P. W. Fowler, Four- and two-electron rules for diatropic and paratropic ring currents in monocyclic π systems. *Chem. Commun.* 2220–2221 (2001).

[44] M. S. Anis *et al,* Qiskit: An open-source framework for quantum computing (2021), 10.5281/zenodo.2573505

[45] F. J. Giessibl, High-speed force sensor for force microscopy and profilometry utilizing a quartz tuning fork. *Appl. Phys. Lett.* **73**, 3956–3958 (1998).

[46] T. R. Albrecht, P. Grütter, D. Horne, D. Rugar, Frequency modulation detection using high-Q cantilevers for enhanced force microscope sensitivity. *J. Appl. Phys.* **69**, 668–673 (1991).

[47] L. Palatinus, G. Chapuis. *SUPERFLIP* – a computer program for the solution of crystal structures by charge flipping in arbitrary dimensions. *J. Appl. Cryst*. **40**, 786–790 (2007).

[48] P. Parois, R. I. Cooper, A. L. Thompson. Crystal structures of increasingly large molecules: meeting the challenges with CRYSTALS software. *Chem. Cent. J.* **9**, 30 (2015).

[49] R. I. Cooper, A. L. Thompson, D. J. Watkin. *CRYSTALS* enhancements: dealing with hydrogen atoms in refinement. *J. Appl. Cryst.* **43**, 1100–1107 (2010).

[50] F. Neese, F. Wennmohs, U. Becker, C. Riplinger. The ORCA quantum chemistry program package. *J. Chem. Phys.* **152**, 224108 (2020).

[51] I. Fdez. Galván *et al.* OpenMolcas: From source code to insight. *J. Chem. Theory Comput.* **15**, 5925–5964 (2019).

[52] C. Riplinger, F. Neese, An efficient and near linear scaling pair natural orbital based local coupled cluster method. *J. Chem. Phys.* **138**, 034106 (2013).

[53] M. J. Frisch *et al.* Gaussian16. (Wallingford, CT, 2016).

[54] F. Weigend, R. Ahlrichs, Balanced basis sets of split valence, triple zeta valence and quadruple zeta valence quality for H to Rn: Design and assessment of accuracy. *Phys. Chem. Chem. Phys.* **7**, 3297–3305 (2005).

[55] P.-O. Widmark, P.-K. Malmqvist, B. R. O. Roos, Density matrix averaged atomic natural orbital (ANO) basis sets for correlated molecular wave functions. *Theor. Chim. Acta* **77**, 291–306 (1990).

[56] J. P. Perdew, K. Burke, M. Ernzerhof. Generalized gradient approximation made simple, *Phys. Rev. Lett.* **77**, 3865–3868 (1996).

[57] S. Grimme, J. Antony, S. Ehrlich, H. Krieg. A consistent and accurate ab initio parametrization of density functional dispersion correction (DFT-D) for the 94 elements H-Pu, *J. Chem. Phys.* **132**, 154104 (2010).

[58] G. Kresse, J. Hafner. *Ab initio* molecular dynamics for liquid metals. *Phys. Rev. B: Condens. Matter Mater. Phys.* **47**, 558–561 (1993).

[59] G. Kresse, J. Hafner. *Ab initio* molecular-dynamics simulation of the liquid–metal–amorphous-semiconductor transition in germanium. *Phys. Rev. B: Condens. Matter Mater. Phys.* **49**, 14251–14269 (1994).

[60] L. Gross, B. Schuler, F. Mohn, N. Moll, N. Pavliček, W. Steurer, I. Scivetti, K. Kotsis, M. Persson, G. Meyer. Investigating atomic contrast in atomic force microscopy and Kelvin probe force microscopy on ionic systems using functionalized tips. *Phys. Rev. B* **90**, 155455 (2014).

[61] G. V. Baryshnikov, R. R. Valiev, R. T. Nasibullin, D. Sundholm, T. Kurten, H. Ågren. Aromaticity of even-number cyclo[*n*]carbons (n = 6–100). *J. Phys. Chem. A* **124**, 10849–10855 (2020).

[62] G. V. Baryshnikov, R. R. Valiev, A. V. Kuklin, D. Sundholm, H. Ågren, Cyclo[18]carbon: insight into electronic structure, aromaticity, and surface coupling. *J. Phys. Chem. Lett.* **10**, 6701–6705 (2019).

[63] I. Schapiro, K. Sivalingam, F. Neese, Assessment of n-electron valence state perturbation theory for vertical excitation energies. *J. Chem. Theory Comp.* **9**, 3567–3580 (2013).

[64] J.-D. Chai, M. Head-Gordon, Long-range corrected hybrid density functionals with damped atom–atom dispersion corrections. *Phys. Chem. Chem. Phys.* **10**, 6615–6620 (2008).

[65] G. V. Baryshnikov, R. R. Valiev, L. I. Valiulina, A. E. Kurtsevich, T. Kurtén, D. Sundholm, M. Pittelkow, J. Zhang, H. Ågren, Odd-number cyclo[*n*]carbons sustaining alternating aromaticity. *J. Phys. Chem. A* **126**, 2445–2452 (2022).

[66] S. Kozuch, J. M. L. Martin, DSD-PBEP86: in search of the best double-hybrid DFT with spin-component scaled MP2 and dispersion corrections. *Phys. Chem. Chem. Phys.* **13**, 20104–20107 (2011).

[67] G. Monaco, F. F. Summa, R. Zanasi, Program package for the calculation of origin-independent electron current density and derived magnetic properties in molecular systems. *J. Chem. Inf. Model*. **61**, 270−283 (2021).

[68] NBO Version 3.1, E. D. Glendening, A. E. Reed, J. E. Carpenter, F. Weinhold.

[69] K. Remya, C. H. Suresh. Carbon rings: a DFT study on geometry, aromaticity, intermolecular carbon–carbon interactions and stability, *RSC Adv.* **6**, 44261–44271 (2016).

Acknowledgments: We thank the following organizations for support:

European Research Council grant 885606, ARO-MAT (HLA, YG)

European Community Horizon 2020 grant CycloCarbonCatenane (YG, HLA)

European Community grant ElDelPath (IR, HLA)

Leverhulme Trust (Project Grant RPG-2017-032) (HLA, LMS)

European Research Council Synergy grant MolDAM (grant number 951519) (LG, FA)

European Union project SPRING (grant number 863098) (LG, SM)

Computational resources were provided by:

Cirrus UK National Tier-2 HPC Service at EPCC (http://www.cirrus.ac.uk) funded by the University of Edinburgh and EPSRC (EP/P020267/1)

Ministry of Education, Youth and Sports of the Czech Republic through the e-INFRA CZ (ID:90140)

Author contributions:

Conceptualization: HLA and LG

Synthesis of precursors: YG, IE, PK, LMS and HLA

Atom manipulation and scanning probe microscopy: FA and LG

Theory and computational simulation: IR, LR, MR and IT

Crystal structure determination of compound **6**: KEC

Supervision: HLA, LG and IT

Writing – original draft: YG, FA, IR, HLA and LG

Writing – review & editing: all authors

Competing interests: The authors declare that they have no competing interests.

Data and materials availability: All data are available in the main text or the supplementary materials.